

# ULRR

## A high figure of merit vibrational energy harvester for low frequency applications

Item Type	Article
Authors	Nico, Valeria;Boco, Elisabetta;Frizzell, Ronan;Punch, Jeff
Citation	Applied Physics Letters;108:013902
Publisher	American Institute of Physics
Download date	2026-04-17 22:04:47
Item License	<a href="https://creativecommons.org/licenses/by-nc-sa/1.0/">https://creativecommons.org/licenses/by-nc-sa/1.0/</a>
Link to Item	<a href="https://hdl.handle.net/10344/6333">https://hdl.handle.net/10344/6333</a>

## A high figure of merit vibrational energy harvester for low frequency applications

V. Nico,<sup>1</sup> E. Boco,<sup>1</sup> R. Frizzell,<sup>2</sup> and J. Punch<sup>1</sup>

<sup>1</sup>CONNECT, Stokes Laboratories, University of Limerick, Ireland

<sup>2</sup>Efficient Energy Transfer ( $\eta$ ET) Department, Bell Labs, Alcatel-Lucent, Dublin, Ireland

(Received 4 November 2015; accepted 15 December 2015; published online 6 January 2016)

Small-scale vibration energy harvesters that respond efficiently at low frequencies are challenging to realize. This paper describes the design and implementation of one such harvester, which achieves a high volumetric Figure of Merit ( $FoM_v = 2.6\%$  at 11.50 Hz) at the scale of a C-type battery and outperforms other state-of-the-art devices in the sub 20 Hz frequency range. The device employs a 2 Degree-of-Freedom velocity-amplified approach and electromagnetic transduction. The harvester comprises two masses oscillating one inside the other, between four sets of magnetic springs. Collisions between the two masses transfer momentum from the heavier to the lighter mass, exploiting velocity amplification. The paper first presents guidelines for designing and optimizing the transduction mechanism, before a nonlinear numerical model for the system dynamics is developed. Experimental characterisation of the harvester design is then presented to validate both the transducer optimization and the dynamics model. The resulting high  $FoM_v$  demonstrates the effectiveness of the device for low frequency applications, such as human motion. © 2016 AIP Publishing LLC. [<http://dx.doi.org/10.1063/1.4939545>]

Wireless sensor networks are currently widespread in many aspects of everyday life.<sup>1</sup> Typically, each sensor is independently powered by batteries, which potentially leads to some major issues: batteries have a limited lifetime, and their disposal is polluting. Moreover, their replacement in a large network can be costly due to their high numbers and practically difficult, because they may be embedded in structures, and so difficult to reach.<sup>2</sup> Battery limitations have led to the interest in converting energy which is already present in the environment into electrical energy. Among all the possible sources, kinetic energy from ambient vibrations is one of the most common forms. Conventional Vibrational Energy Harvesters (VEHs) are based on simple linear spring-mass resonator designs, for which the resonant frequency of the device has to be tuned to the dominant frequency of the ambient vibration. To overcome this problem, a 2 Degree-of-Freedom (2DoF) electromagnetic velocity amplified VEH is presented in this paper. These configurations have been shown to naturally enhance the frequency response and power generated in VEHs due to the nonlinear effects introduced by impacts within the device, which enable momentum transfer between masses.<sup>3–8</sup> To enable effective operation at the low frequencies typical of human motion applications (typically under 5 Hz), a nonlinear contribution to the system dynamics of the device described in this paper was added through the use of magnetic springs. Such an approach results in an efficient but small-scale VEH device that couples the high power and wide frequency response of the velocity amplified VEHs but enables operation at low frequencies and leads to high volumetric Figure of Merit ( $FoM_v$ ) values that outperform recently published results ( $FoM_v = 2.6\%$  at 11.5 Hz).

This paper outlines a design methodology to electrically optimize the harvester. A numerical model for predicting the dynamics of the device is then presented before the  $FoM_v$  is calculated and compared with recently published results.

The aim of this study is to design a small-scale 2DoF velocity amplified VEH that responds effectively at low frequencies. C-battery scale was chosen, since it is a commonly used volume for batteries that can readily be integrated in machinery, or portable devices. In order to achieve high energy density, the configuration presented in Fig. 1 was chosen, which consists of a larger primary mass (Mass 1) made up of seven coils that oscillates vertically between two sets of opposing NdFeB magnets (on the top and bottom of the external housing), forming magnetic springs.

The primary mass surrounds a smaller secondary mass (Mass 2), made up of a stack of five magnets, moving itself between two sets of weaker magnetic springs inside the primary mass. The collisions between the two masses exploit velocity amplification, which is highly advantageous for electromagnetic energy harvesting.<sup>4,6,8,9</sup> The choice of cap height ( $H$ ) can modify the spectral behavior of the device, as this varies the distance between the opposing magnets that

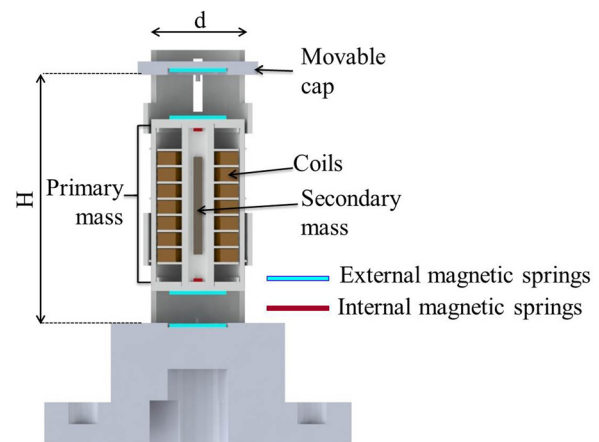


FIG. 1. Cross section of the harvester, illustrating the two masses that oscillate one inside the other.

form the outer magnetic springs. The presence of magnetic springs leads to strong nonlinear behavior, which is highly valuable for energy harvesting, as it allows the bandwidth to be increased and enables low resonant frequencies to be achieved with reduced volume penalty compared to what is achievable with mechanical springs.<sup>10–14</sup>

In order to design an optimized system, the first aim was to achieve the best possible magnetic field density. A classical stack of magnets (Fig. 2(a)) has a strong magnetic field on the opposing poles but almost zero strength along the stack length. For a coil wrapped around the stack, the induced electromotive force (e.m.f) will be very low (since  $e.m.f. = -d\phi/dz$ , where  $\phi$  is the magnetic flux). In Fig. 2(b), a Halbach configuration is presented: it consists of an array of alternating axially polarized and diametrically polarized magnets.<sup>15,16</sup> The magnetic field is very low on the top and bottom sides of the stack. On one side of the length, assuming an infinite ideal stack, the amplitude of the field oscillates as  $H(x, y) = H_0 e^{ikx} e^{-ky}$ , where  $H_0$  is the field amplitude on the array surface and  $k = 2\pi/\lambda$ , where  $\lambda$  is the wavelength of the oscillation. On the other side, the field cancels due to interference.<sup>17,18</sup>

The benefit of this approach is that the flux lines close and double the magnetic field intensity in regions where radial and axial magnetic fields intersect. This configuration allows more current to be generated for small displacements of the magnets compared to the classical stack and was therefore chosen as the most suitable for harvesting energy from low amplitude excitations. In order to harvest energy efficiently, a system of seven coils was employed, each one with the same thickness of the magnets height. They were not chosen to be smaller (as in Ref. 15) due to practical winding issues.

To determine the optimum number of turns for each coil, the VEH was considered, to a first approximation, as a spring-mass-damper system, in which the damping is both due to the mechanical losses and to the conversion method. It is well known that for an harmonic forced damped oscillator the power output dissipated at resonance ( $P(\omega_N)$ ) by the electromagnetic damping only follows:<sup>19</sup>

$$P(\omega_N)_{em} = \frac{mY^2\omega^3\xi_{em}}{4(\xi_{em} + \xi_{mech})^2}, \quad (1)$$

where  $Y$  is the amplitude of the excitation,  $\xi_{mech}$  and  $\xi_{em}$  are, respectively, the mechanical and electromagnetic damping, and  $m$  is the mass of the device. Differentiating Eq. (1) and equating to zero shows that the maximum power is dissipated through the electromagnetic damping if  $\xi_{em} = \xi_{mech}$ .

Therefore, it was necessary to determine the number of turns ( $N$ ) for each of the coils that resulted in equal electromagnetic and mechanical damping. To achieve this condition, a series of standard drop tests were carried out to determine the mechanical damping ( $\gamma_{mech} = 0.011$  Ns/m) and the mean magnetic field for the system ( $B = 0.017$  T). An algorithm was then implemented that found the optimum  $N$  for four different wire diameters by determining the electromagnetic damping for varying  $N$  and equating this to the mechanical damping. Finally, for each optimal  $N$ , the final coil radius was estimated considering the thickness of the wire and the number of turns, to ensure that the volumetric constraints of the device were not violated. The optimum set of coils, which met the volumetric constraints, was found to have  $N = 2800$  turns each, wound with  $50 \mu\text{m}$  diameter wire.

It was necessary to verify that the coil parameters found using the methods outlined above resulted in optimal power generation for a range of cap heights. Three coils were tested, each having the same wire diameter but different numbers of turns, and each coil was tested for three different cap heights (i.e., varying  $H$  in Fig. 1).

The device was mounted on an LDS V406 permanent magnet shaker from Bruel&Kjaer, which was controlled by LabView. The acceleration given by the shaker was measured by a high sensitivity ( $101.4$  mV/g,  $g = 9.81$  m/s<sup>2</sup>) PCB Piezotronic accelerometer which was used as feedback to ensure the acceleration was constant for the range of excitation frequencies tested. The voltage output was measured and recorded in Labview using a NI-DAQ card across a known resistance, which was changed for the different sets of coils, in order to obtain the maximum power output. The weight of the larger mass was kept constant for all coils, by adding appropriate amount of copper masses. Data using  $H = 50.10$  mm,  $52.40$  mm, and  $57.45$  mm were recorded at a fixed acceleration of  $0.4$  g, which ensured good dynamical behaviour for the device. In Fig. 3, the comparison between the three sets of coils at three different  $H$  is shown: for each  $H$  tested, although the voltage output increased with greater

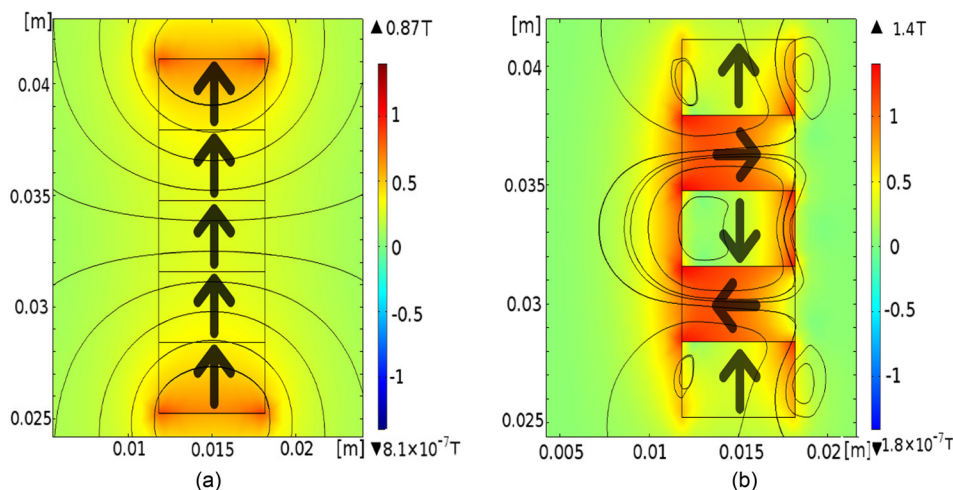


FIG. 2. Magnetic field density for the two magnet configurations. The field lines are sketched in black. The colour scale refers to the amplitude of the magnetic field density in [T]. Arrows indicate the polarization. (a) Classical stack of magnets and (b) Halbach configuration.

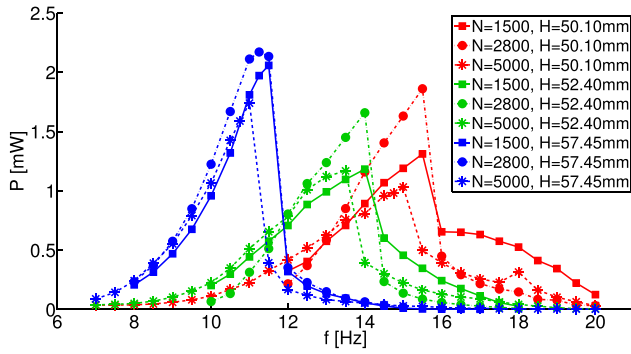


FIG. 3. Power output comparisons for the three sets of coils with changing cap height.

number of turns, the power output reached its maximum for  $N = 2800$  turns in each coil, which correlated with the linear theory prediction of the above paragraph.

The enhanced power output for the higher cap heights is most likely due to the increased nonlinear contribution given by velocity amplification of the larger mass: when the cap was higher, the magnetic spring forces did not affect the outer mass as strongly in comparison to the cases where the cap height was lower. This allowed the larger mass to oscillate more freely following impact with the harvester base. Consequently, the masses gained higher relative velocities following impact events when the cap was higher, leading to higher power (since  $P_{em} \propto v^2$  (Refs. 4–9)).

Changes in the relative performance of optimal and non-optimal conditions can be seen in Fig. 3 for the different cap heights: at lower cap heights, the coil type has a larger effect on the performance of the system than when the cap is at its highest point. This is most likely caused by the fact that the power generated by the system is limited by the available displacement range of the masses. Thus, the system performance can saturate for given excitation conditions and leads to the three coil types performing similarly for the  $H = 57.45$  mm case. Increasing the cap height beyond  $H = 57.45$  mm would be expected to give even less variation in the performance of the different coils.

In this section, a theoretical model which describes the system dynamics is developed. The device described in the above paragraph can be modeled as two masses moving one inside the other, connected by magnetic springs. An acceleration  $\ddot{y}$  is applied to the system, and the masses can only move vertically. Finite element simulation of the NdFeB magnets forming the magnetic springs was carried out using COMSOL Multiphysics in order to evaluate the variation of the repulsive magnetic force with distance. According to Ref. 20, the magnetic force as a function of distance has been fitted with

$$F_{mag} = \frac{p_1}{x^4 + q_1x^3 + q_2x^2 + q_3x + q_4}, \quad (2)$$

where  $x$  is the distance between the magnets and  $p_1, q_1, q_2, q_3, q_4$  are fitting parameters. The root mean squared error of the fit was  $RMSE = 0.087$ .

The system behavior can be represented by three coupled nonlinear differential equations: two of which

describe the dynamics of the masses, and one the electrical output of the coil

$$\begin{cases} m_1 \ddot{z}_1 = -(d_1 + d_2)\dot{z}_1 + F_{mag} - F_{mag2} - F_{int} + F_{int1} \\ \quad + d_2\dot{z}_2 - m_1\ddot{y} - m_1g \\ m_2 \ddot{z}_2 = -d_2\dot{z}_2 + F_{int} - F_{int1} + d_2\dot{z}_1 - \alpha V_L - m_2\ddot{y} \\ \quad - m_2g \\ \dot{V}_L = \delta_c \omega_c (\dot{z}_2 - \dot{z}_1) - \frac{R_L + R_c}{L_c} V_L, \end{cases} \quad (3)$$

where  $z_1$  and  $z_2$  are the displacements of the two masses;  $F_{mag}$ ,  $F_{mag2}$ ,  $F_{int}$ , and  $F_{int1}$  are the repulsive magnetic force of the magnetic springs, given by Eq. (2);  $d_1$  and  $d_2$  are the viscous damping coefficients acting on  $m_1$  and  $m_2$ , measured by exciting the device with a pulse load and examining the transient displacement of the masses;  $\alpha = B/R_L$  is the conversion factor; and  $\alpha V_L$  is the magnetic force due to the transduction mechanism.

The Halbach stack of magnets was considered as one single magnet, the magnetic field was calculated from the electromagnetic damping measurements, and the seven coils were considered as one single coil with total  $N$ , resistance and inductance set equal to the respective sums from the individual coils.

The three differential equations were solved numerically using the Runge-Kutta algorithm in order to predict the output power over a range of frequencies for different acceleration levels and three cap heights. Fig. 4 shows the predicted output power for the  $N = 2800$  coils that, according to the above paragraph, is the optimal set of coils. The behavior of the system is influenced by  $H$ : the resonance frequency shifts to higher values when  $H$  is decreased (similar to the results in Fig. 3).

This is mainly a result of the hardening effect of the magnetic springs: decreasing the distance between the opposing magnets increases the effective elastic coefficient. A similar effect is evident when increasing the acceleration for fixed  $H$ : the peak at  $a_{rms} = 0.2$  g is almost symmetric, while at  $a_{rms} = 0.4$  g the peak is shifted to a higher frequency and becomes asymmetric, bending to the right. This is due to the fact that at higher acceleration, the larger mass can reach

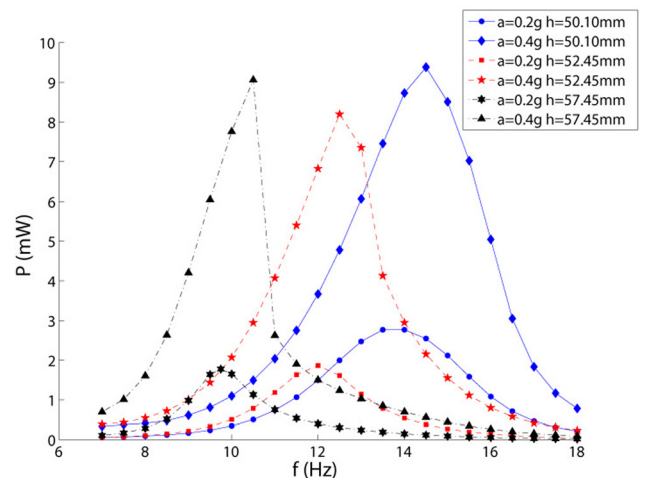


FIG. 4. Theoretical trend of the output power as a function of frequency for different excitations and cap heights.

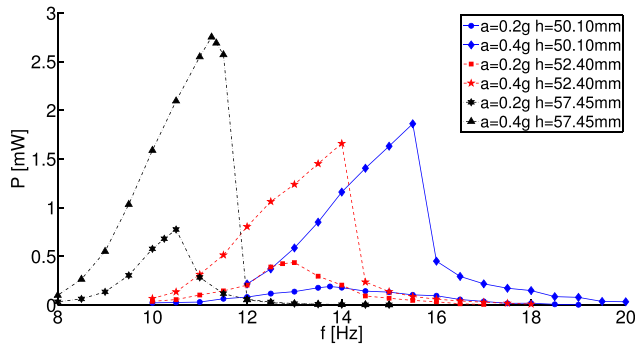


FIG. 5. Experimentally measured output power as a function of frequency for different accelerations and  $H$ .

positions closer to the top magnets, resulting in an increase of the effective elastic constant acting on the masses.

The output power over a range of frequencies for the three different values of  $H$  and the  $N=2800$  coils were measured experimentally, and the results are shown in Fig. 5. The device was tested under sinusoidal excitation at  $a_{rms}=0.2$  g and  $a_{rms}=0.4$  g. The maximum measured output power is  $P=2.75$  mW at  $a_{rms}=0.4$  g and  $f=11.25$  Hz. The results shown in Fig. 5 demonstrate similar trends to those predicted by the theoretical model in Fig. 4. Specifically, the shifting of the resonant point to lower frequencies with increasing  $H$  and the asymmetric hardening effect with increased acceleration for a given  $H$  are evident in both theoretical and experimental investigations. The correlation between experimental and theoretical results suggests that the model is a useful tool for tuning the harvester to the main frequency of the ambient vibrations. It is noted, however, that the predicted peak power does not compare well to the experimental results, and this is most likely due to the simplifying assumptions made in modeling the Halbach stack and the seven coils discussed previously.

The performance of the harvester has been compared with devices reported in recent literature, using the  $FoM_v$ ,<sup>21</sup> defined as

$$FoM_v = \frac{P_{out}}{\frac{1}{16} Y_0 \rho_{Au} Vol^{\frac{4}{3}} \omega^3}, \quad (4)$$

where  $P_{out}$  is the output power,  $Y_0$  is the input displacement amplitude,  $\omega$  is the radial frequency of the excitation,  $\rho_{Au}$  is the density of gold, and  $Vol$  is the harvester volume. Table I reports the  $FoM$  calculated for the three different coils presented in the above paragraph using the configuration with  $H=57.45$  mm. The device volume employed in this calculation changed since  $N$  for each coil varied and resulted in coils of different radial dimensions. The outer housing could,

TABLE I.  $FoM_v$  for the three different coils considered in the previous paragraphs.

Coil	Volume (cm <sup>3</sup> )	Frequency (Hz)	Acceleration (g)	Power (mW)	$FoM_v$ (%)
5000-turn	29.30	11.00	0.4	1.74	0.42
2800-turn	12.10	11.25	0.4	2.75	2.08
1500-turn	8.12	11.50	0.4	2.06	2.60

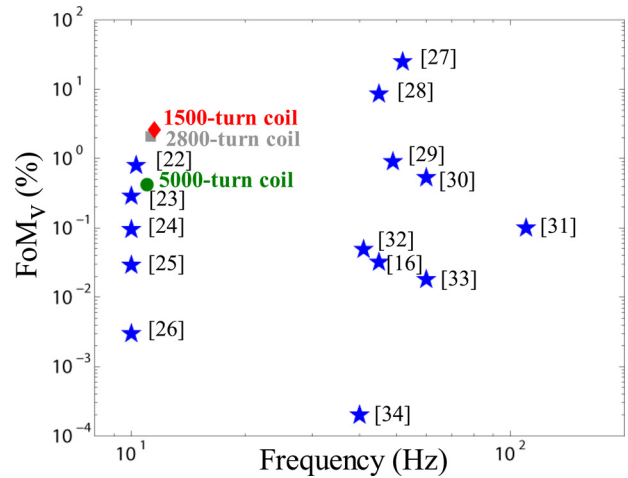


FIG. 6. Comparison between recently published  $FoM_v$ .<sup>16,22–34</sup> Reproduced with permission from Ashraf *et al.*, Sens. Actuators A **195**, 123 (2013). Copyright 2013 Elsevier.

therefore, be sized to encompass the different coils more closely, and this resulted in variations in the overall volume of the device.

Fig. 6 shows how the values of the  $FoM_v$  listed in Table I compare with recently reported harvesters. The high value of  $FoM_v=2.6\%$  is an important result as it demonstrates the effectiveness of employing the principle of velocity amplification in an electromagnetic VEH for low frequencies applications.

Small volume harvesters are often considered unsuitable for achieving high  $FoM_v$  values since they limit the relatively large amplitude oscillations normally associated with low frequency vibrations.<sup>22</sup> In addition, increasing the inertial mass of a harvester to reduce the resonant point is not always possible without violating volume or cost constraints. The high  $FoM_v$  values in Fig. 6 are a result of the greater power output associated with the amplified velocity of the secondary mass, which is a direct result of the momentum transfer following impacts with the larger mass.<sup>5,9</sup>

In this paper, a high performance vibration energy harvester for low frequency applications has been presented, which achieves volumetric figure of merit values that outperform state-of-the-art devices in the sub 20 Hz range. The harvester design was based on a nonlinear 2DoF approach that employs velocity amplification. This approach allowed the harvester to maintain a relatively high power output within a constrained volume and enabled the device to respond well at low frequencies.

The paper describes the use of a Halbach stack of magnets and the optimisation of the surrounding coils. The effect of variations in applied acceleration and cap height were investigated numerically and experimentally to explore the performance of the device and to demonstrate its effectiveness for low frequency applications such as human motion.

The authors acknowledge the financial support of Science Foundation Ireland under Grant No. 10/CE/I1853 and the Irish Research Council (IRC) for funding under their Enterprise Partnership Scheme (EPS). Bell Labs Ireland

would also like to thank the Industrial Development Agency (IDA) Ireland for their continued support.

- <sup>1</sup>M. Pickavet, W. Vereecken, S. Demeyer, P. Audenaer, B. Vermeulen, C. Develder, D. Colle, B. Dhoedt, and P. Demeester, in *2nd International Symposium on Advanced Networks and Telecommunication Systems, 2008, ANTS'08* (2008), p. 1.
- <sup>2</sup>I. A. Kollias, in Proceedings of SMARTGREENS 2014, Sustainable Computing and Communications (2014).
- <sup>3</sup>R. L. Waters, B. Chisum, H. Jazo, and M. Fralick, in Nanopower Forum 2008 (2008).
- <sup>4</sup>V. Nico, D. O'Donoghue, R. Frizzell, G. Kelly, and J. Punch, *Proc. ASME* **2**, V002T07A011 (2014).
- <sup>5</sup>E. Boco, V. Nico, D. O'Donoghue, R. Frizzell, G. Kelly, and J. Punch, in Proceedings of SMARTGREENS 2015 Conference (2015).
- <sup>6</sup>D. O'Donoghue, V. Nico, R. Frizzell, G. Kelly, and J. Punch, *Proc. ASME* **2**, V002T07A010 (2014).
- <sup>7</sup>F. Cottone, S. Goyal, and J. Punch, U.S. patent US8350394 B2 (September 30, 2009).
- <sup>8</sup>F. Cottone, R. Frizzell, S. Goyal, G. Kelly, and J. Punch, *J. Intell. Mater. Syst. Struct.* **25**, 443 (2014).
- <sup>9</sup>V. Nico, E. Boco, R. Frizzell, and J. Punch, in Proceedings of SMASIS2015 (2015).
- <sup>10</sup>M. Mizuno and D. G. Chetwynd, *J. Micromech. Microeng.* **13**, 209–216 (2003).
- <sup>11</sup>G. Rebeiz, G. W. Regehr, D. B. Rutledge, R. L. Savage, and L. Richard, *Int. J. Infrared Millimeter Waves* **8**, 1249 (1987).
- <sup>12</sup>H. Wu, L. Tang, Y. Yang, and C. K. Soh, *J. Intell. Mater. Syst. Struct.* **24**, 357 (2013).
- <sup>13</sup>H. Wu, L. Tang, Y. Yang, and C. K. Soh, *J. Intell. Mater. Syst. Struct.* **25**, 1875–1889 (2014).
- <sup>14</sup>S.-J. Jang, E. Rustighi, M. J. Brennan, Y.-P. Lee, and H.-J. Jung, *J. Intell. Mater. Syst. Struct.* **22**, 443 (2011).
- <sup>15</sup>X. Tang, T. Lin, and L. Zuo, *IEEE/ASME Trans. Mechatronics* **19**, 615 (2014).
- <sup>16</sup>D. Zhu, S. Beeby, J. Tudor, and N. Harris, *Smart Mater. Struct.* **21**, 075020 (2012).
- <sup>17</sup>K. Halbach, *Nucl. Instrum. Methods* **169**, 1 (1980).
- <sup>18</sup>J. Mallinson, *IEEE Trans. Magn.* **9**, 678 (1973).
- <sup>19</sup>S. P. Beeby, M. J. Tudor, R. N. Torah, E. Koukharenko, T. O'Donnell, and S. Roy, in Proceedings of DTIP of MOEMS and MEMS, Stresa, Italy (2006).
- <sup>20</sup>Y. Kraftmakherl, *Eur. J. Phys.* **28**, 409 (2007).
- <sup>21</sup>P. D. Mitcheson, E. M. Yeatman, G. K. Rao, A. S. Holmes, and T. C. Green, *Proc. IEEE* **96**, 1457 (2008).
- <sup>22</sup>K. Ashraf, M. H. Khir, J. O. Dennis, and Z. Baharudin, *Sens. Actuators A* **195**, 123 (2013).
- <sup>23</sup>K. Ashraf, M. H. Khir, J. O. Dennis, and Z. Baharudin, *Smart Mater. Struct.* **22**, 025018 (2013).
- <sup>24</sup>T. V. Galchev, J. Cullagh, R. L. Peterson, and K. Najafi, *J. Micromech. Microeng.* **21**, 104005 (2011).
- <sup>25</sup>T. Galchev, H. Kim, and K. Najafi, *Procedia Chem.* **1**(1), 1439–1442 (2009).
- <sup>26</sup>M. Renaud, P. Fiorini, R. V. Schaijk, and C. V. Hoof, *Smart Mater. Struct.* **18**, 035001 (2009).
- <sup>27</sup>S. P. Beeby, R. N. Torah, M. J. Tudor, P. Glynne-Jones, T. O'Donnell, C. R. Saha, and S. Roy, *J. Micromech. Microeng.* **17**, 1257 (2007).
- <sup>28</sup>I. N. Ayala, D. Zhu, M. J. Tudor, and S. P. Beeby, in *PowerMEMS* (2009), pp. 49–52.
- <sup>29</sup>D. F. Berdy, P. Srisungsithisunti, X. Xu, F. Rhoads, B. Jung, and D. Peroulis, in *PowerMEMS* (2009).
- <sup>30</sup>See <http://www.ferrosi.com/files/VEH460.May09.pdf> for Ferro Solutions VEH-460.
- <sup>31</sup>N. H. Ching, H. Y. Wong, J. Li, H. W. Leong, and Z. Wen, *Sens. Actuators A* **97–98**, 685 (2002).
- <sup>32</sup>E. Sardini and M. Serpelloni, *Sens. Actuators A* **172**, 475 (2011).
- <sup>33</sup>S. Kulkarni, E. Koukharenko, R. Torah, J. Tudor, S. Beeby, T. O'Donnell, and S. Roy, *Sens. Actuators A* **145–146**, 336 (2008).
- <sup>34</sup>B. Yang and C. Lee, *Microsyst. Technol.* **16**, 961–966 (2010).